

3C 48: Stellar Populations and the Kinematics of Stars and Gas in the Host Galaxy¹

Gabriela Canalizo² and Alan Stockton²

Institute for Astronomy, University of Hawaii, 2680 Woodlawn Drive, Honolulu, HI 96822

ABSTRACT

We present deep Keck LRIS spectroscopy of the host galaxy of 3C 48. Our observations at various slit positions sample the different luminous components near the quasar, including the apparent tidal tail to the NW and several strong emission line regions.

By fitting Bruzual & Charlot (1996) population synthesis models to our spectra, we obtain ages for the most recent major episodes of star formation in various parts of the host galaxy covered by our slits. There is vigorous current star formation in regions just NE and SE of the quasar and post-starburst regions with ages up to 10^8 years in other parts of the host galaxy, but most of the NW tidal tail shows no sign of significant recent star formation. We use these model fits, together with the kinematics of the stars and gas, to outline a plausible evolutionary history for the host galaxy, its recent starburst activity, the triggering of the quasar, and the interaction of the radio jet with the ambient gas.

There is strong evidence that the 3C 48 host is an ongoing merger, and that it is probably near the peak of its starburst activity. Nevertheless, the quasar itself seems to suffer little extinction, perhaps because we are viewing it along a particularly favorable line-of-sight.

Subject headings: galaxies: interactions | galaxies: infrared | galaxies: starburst | galaxies: jets | quasars: individual (3C 48)

¹Based on observations made with the NASA/ESA Hubble Space Telescope, obtained from the data archive at the Space Telescope Science Institute, which is operated by the Association of Universities for Research in Astronomy, Inc., under NASA contract NAS 5-26555.

²Visiting Astronomer, W. M. Keck Observatory, jointly operated by the California Institute of Technology and the University of California.

1. Introduction

Strong interactions and mergers have been implicated in the triggering of both ultra-luminous infrared galaxies (ULIGs; Sanders et al. 1988; Sanders & Mirabel 1996 and references therein) and QSOs (e.g., Stockton 1999 and references therein). For ULIGs with the highest FIR luminosities ($\log L_{\text{FIR}} > 12.0$ in solar units), essentially all appear to be mergers. The evidence linking interactions to QSOs, while strong for a number of specific cases, is generally more circumstantial and less compelling than that for ULIGs. This does not necessarily imply lower interaction rates for QSO host galaxies: it is much more difficult to observe diagnostic features in QSO hosts because of the bright nucleus. Sanders et al. (1988) have suggested that there may be an evolutionary path from ULIGs to QSOs. If so, then signs of the interaction also would be expected to be less obvious in QSOs because of the fading and dissipation of tidal features such as tails.

The relation of mergers to intense starbursts (resulting in ULIGs) and to the feeding of supermassive black holes (resulting in QSO activity) is undoubtedly complex. Some mergers of disk galaxies result in only comparatively moderate star formation, and most mergers apparently do not lead to strong nuclear activity. It is not yet clear whether the extra ingredients (besides the bare fact of a merger) needed to produce a sizable starburst are necessarily identical to those required to trigger strong nuclear activity, but the fact that a fair fraction of ULIGs show signs of nuclear activity indicates that there is at least a good deal of overlap. In order to explore this connection in more detail, we have initiated a program to study stellar populations in the host galaxies of QSOs having FIR colors tending towards those of ULIGs, and therefore indicating a substantial contribution from a starburst or recent post-starburst component. We have previously fitted population-synthesis models to high-S/N spectroscopy of the close, interacting companion to the QSO PG 1700+518 (Canalizo & Stockton 1997; Stockton, Canalizo, & Close 1998). Here, we use similar techniques to analyze the host galaxy of 3C 48.

3C 48 was the first quasar to be discovered (Matthews et al. 1961; Matthews & Sandage 1963). As often seems to be the case for the first example of a new class of astronomical object, it is, in retrospect, far from being typical. The original identification of 3C 48 depended in part on the small size of its radio source, and it remains the only example of a compact steep-spectrum (CSS) radio source among powerful quasars at redshifts < 0.5 . The host galaxy of 3C 48 is unusually large and bright in comparison with those of other low-redshift quasars (Kristian 1973). 3C 48 was the first QSO for which an extended distribution of ionized gas was observed (Wampler et al. 1975), and it remains one of the most luminous examples of extended emission among low-redshift QSOs (Stockton & Mackenty 1987).

Spectroscopy of the host galaxy of 3C 48 by Boroson & Oke (1982, 1984) showed strong Balmer absorption lines, demonstrating clearly not only that the extended continuum radiation was dominated by stars, but that these stars were fairly young (< 1 Gyr old). A similar story is told by the far-infrared (FIR) colors, which lie between those of most QSOs and those of ULIGs, indicating that a significant fraction of the FIR radiation is likely due to dust in regions of current or recent star formation (Neugebauer et al. 1986; Stockton & Ridgway 1991; Stockton 1999). Another connection with ULIGs is seen in the apparent tidal tail extending to the northwest from the 3C 48 host galaxy and the possibility that the luminosity peak 1⁰ northeast of the quasar nucleus might be the nucleus of a merging companion (Stockton & Ridgway 1991).

In this paper, we describe the results of deep spectroscopy of the host galaxy of 3C 48, using multiple slit positions to cover most regions of the galaxy. After analyzing the stellar velocity field, fitting population-synthesis models to the spectra at many discrete points in the host galaxy, and determining the distribution and velocity structure of the extended emission-line gas, we discuss the implications of our results in terms of a merger scenario. We assume $H_0 = 75 \text{ km s}^{-1} \text{ Mpc}^{-1}$ and $q_0 = 0.5$ throughout this paper.

2. Observations and Data Reduction

Spectroscopic observations of the host galaxy of 3C 48 were carried out on 1996 October 13{14 UT and 1996 November 3{4 UT, with the Low-Resolution Imaging Spectrometer (LRIS; Oke et al. 1995) on the Keck II telescope. In Table 1 we show a complete journal of observations, with specification of the slit positions. We used a 600 groove mm^{-1} grating blazed at 5000 Å for slit positions A, B, C, and G, yielding a dispersion of $1.28 \text{ Å pixel}^{-1}$. We used a 900 groove mm^{-1} grating blazed at 5500 Å for the remaining slit positions in order to obtain a higher dispersion ($0.85 \text{ Å pixel}^{-1}$) to observe the structure of the emission lines in the spectra. Total integration times were 5 minutes for slit position D, 40 minutes for slit position F, and 60 minutes for all the other slit positions.

The spectra were reduced with IRAF, using standard reduction procedures. After dark, bias and flat field correction, the images were background subtracted to remove sky lines. Wavelength calibrations were made using the least-mean-squares fit of cubic spline segments to identified lines in a comparison spectrum. The spectra were flux calibrated using spectrophotometric standards from Massey et al. (1988) observed with the slit at the parallactic angle. The distortions in the spatial coordinate were removed with the APEXTRACT routines. The spectra were not corrected for discrete atmospheric absorption features; thus they show the atmospheric B-band redwards of the [O III] 5007 emission

feature.

Spectra from slit position A suffered from strong light scattering from the quasar. In addition, one of the three 20 minute exposures taken at this position was unusable because of problems with the Keck II mirror control system.

Spectra from slit positions A, B, C and G were subdivided into eight regions each (see Fig. 1a) for the analysis of stellar populations and kinematics of the host galaxy. The size of each of these regions was chosen so that each spectrum would have sufficient signal-to-noise ratio for modeling while still providing good spatial resolution.

The spectra of regions close to the quasar nucleus were contaminated by scattered quasar light. The scattered light was removed by subtracting from each region a version of the quasar nuclear spectrum, scaled to match the broad-line flux. The percentage in flux (at 4500 Å, rest wavelength) subtracted in each case is listed in column (6) of Table 2. This quantity depends both on the intensity of the quasar profile wings and the surface brightness of the host galaxy in each particular region.

WFC2 images of 3C 48 were obtained from the Hubble Space Telescope (HST) data archive. The images used in this analysis included two 1400 s exposures in the F555W filter and two 1700 s exposures in the F814W filter. In each case, 3C 48 was centered on the PC1 detector. We also used two 1100 s and one 1300 s exposures in the linear ramp filter FR680N, centered on redshifted [O III] 5007. 3C 48 fell near the center of the WFC2 chip. All HST images were reduced as described in Canalizo, Stockton & Roth 1998. We subtracted a scaled stellar profile at the position of the quasar, using Tiny Tim (Krist 1993) models of the HST/WFC2 PSF.

We also use three ground-based images of 3C 48 obtained with the University of Hawaii 2.2 m telescope. The first of these is a sum of three 2700 s exposures, taken on 1991 September 16 with a Tektronix 1024 × 1024 CCD through a 30 Å bandpass filter centered on redshifted [O III] 5007, with an image scale of 0.22 pixel⁻¹. The second is a sum of 30 × 300 s exposures, taken on UT 1993 September 18 with a Tektronix 2048 × 2048 CCD through a filter centered at 6120 Å and having a 960 Å FWHM, covering the relatively line-free region of the rest-frame spectrum from 4120 to 4820 Å in the rest frame of 3C 48, also at a scale of 0.22 pixel⁻¹. We shall refer to this filter as "R⁰". Finally, we obtained short wavelength images of 3C 48 on UT 1998 September 18 through a U⁰ filter (centered at 3410 Å with a 320 Å FWHM). Nine 1200 s exposures were taken using an Orbit CCD, with an image scale of 0.138 pixel⁻¹. All ground-based images were reduced with IRAF using standard image reduction procedures. The U⁰ and R⁰ have been processed with CPLUCY (Hook 1998), an improved version of the PLUCY task (Hook et al. 1994) available in the

STSDAS CONTRIB package. Both tasks carry out a two-channel deconvolution of a field, one channel comprising designated point sources, which are deconvolved using the standard Richardson-Lucy algorithm, and the second channel including everything else, for which the Richardson-Lucy deconvolution is constrained by an entropy term to ensure smoothness. One of the virtues of this procedure is that, with a proper choice of parameters, it is possible to remove the stellar profile from a non-zero background without the ringing problem inherent in the application of the standard Richardson-Lucy procedure.

Both the ground-based images and the HST images are shown in Fig. 2, to which we will refer as needed during our discussion.

3. Results

3.1. Kinematics of the Stellar Component in the Host Galaxy

Redshifts determined from stellar absorption features give us information about the kinematics of the stars in the host galaxy. We have obtained measurements from 32 regions covered by 4 slit positions (A, B, C and G; see Table 1). Some of these regions overlap, providing a consistency check. Column (2) of Table 2 lists the relative velocity of each region with respect to $z = 0.3700$, which is close to the average of the stellar redshifts measured in the inner regions of the host.

Measuring redshifts from stellar absorption features presents two main problems: the absorption features may be contaminated by emission lines coming from the extended ionized gas, and some absorption features may be interstellar in nature.

Contamination of absorption features by emission can yield a higher or lower redshift depending on whether the ionized gas has a lower or higher redshift than the stars. In order to check for contamination, we examined the Balmer lines. Because the Balmer decrement is steeper in emission than in absorption, those lines that are higher in the series (e.g., H 8, H 9, H 10) show less contamination by emission. As a result, in the regions where there is extended emission, the redshift measured from the lower lines in the Balmer series was different from that measured from the higher-series lines. This effect is quite significant in some cases, and it correlates with the strength of the emission observed in our [O III] image (Fig. 2f). Where there was evidence for strong emission contamination, we measured the redshift of the stellar component only from the higher Balmer lines (usually H 8 and above) and the Ca II K line. We did not measure redshifts from Ca II H when a young stellar component was present as this line was blended with H γ .

Redshifts measured from Ca II lines, however, must be treated with caution, as these lines occur often in the interstellar medium. From our modeling of stellar populations (see x 3.2) we notice that Ca II is sometimes stronger in the observed spectrum than in an otherwise good fitting model (e.g., at B4 in Fig. 3), and this is indicative of intervening interstellar gas, which may have a different velocity from that of the stellar component. However, for those spectra with a young stellar component, the redshift we measured from Ca II K was always consistent with that measured from the higher members of the Balmer series within measurement errors. In the cases where there was no young stellar component, we checked for consistency with other old population features, such as the Mg Ib feature.

Figure 1b shows a map of the radial velocities in the host galaxy. The north-west tidal tail-like extension of the host galaxy is blueshifted with respect to the main body of the host galaxy by as much as 300 km s^{-1} . The west end of the tail has smaller approaching velocities ($> 200 \text{ km s}^{-1}$), which increase to a maximum of 300 km s^{-1} , and then decrease again ($\sim 100 \text{ km s}^{-1}$) as we approach the main body of the host. We find relatively small variations in velocity in the central region of the host galaxy. However, the south-east part of the galaxy appears to have receding velocities as high as $+180 \text{ km s}^{-1}$. This may indicate that the system is rotating around an axis oriented roughly northeast-southwest.

3.2. Stellar Populations

3.2.1. Modeling the Spectra

The high signal-to-noise ratio of the Keck LRIS spectra allows us to attempt modeling different regions of the host galaxy, with sizes ranging down to approximately one square arcsecond in the higher-surface-brightness regions. We have modeled 32 individual regions (see Fig. 1b) of the host galaxy using the Bruzual & Charlot 1996 synthesis models.

Typical spectra of the host galaxy are shown in Fig. 3. The spectra generally show Balmer absorption lines from a relatively young stellar population as well as evidence for an older population, such as the Mg Ib feature and the Ca II K line. The simultaneous presence of both kinds of features indicates that we can do some level of decomposition of the two components.

As we shall discuss in more detail in x 4.1, the morphology of the host galaxy indicates that some form of strong interaction has occurred. We assume that this strong tidal interaction has induced one or more major starburst episodes in the host galaxy. Thus, to first order, the observed spectrum consists of an underlying old stellar population (stars in

galaxy before interaction) plus a recent starburst (stars formed as a result of interaction).

Our early experiments in modeling the old population in similar situations showed that, as expected, it is not strongly constrained by the observations. On the other hand, we have found that the precise choice of the underlying old stellar population makes very little difference in the modeling of the superposed starburst (Stockton, Canalizo & Close 1998). Accordingly, we have made what we take to be physically reasonable assumptions regarding the old population and have used this model for all of our analyses. In our early modeling of the central regions of the host galaxy the old stellar component was well fit by a 10 Gyr old population with an exponentially decreasing star formation rate with an e-folding time of 5 Gyr. Later, we were able to extract a purely old population (not contaminated by younger stars) in the tail, far from the nucleus (see C8 in Figs. 1a and 3). The old population model we had previously chosen gives a very reasonable fit, confirming that we had chosen a reasonable model for the old stellar population.

We assume that the same old stellar population is present everywhere in the host galaxy. To this population we add isochrone synthesis models (Bruzual & Charlot 1996) of different ages. The assumption of a population with no age dispersion can be justified if the period during which the star formation rate was greatly enhanced is short compared to the age of the population. Indeed, observational evidence indicates that the duration of starbursts in individual star forming clouds can be very short, often < 1 Myr (e.g., Heckman et al. 1997; Leitherer et al. 1996). We perform a χ^2 fit to the data to determine the contribution of each component and the age of the most recent starburst.

Since the size of each region we are modeling is at least 1×1^0 (4×4 kpc), the observed spectrum is likely to be the integrated spectrum of several starbursts of different ages. The starburst age we derive for the observed spectrum will be weighted towards the younger starbursts because such starbursts will have a greater flux contribution. On the other hand, this weighted-average age will likely be at least somewhat greater than the age of the youngest starburst in the observed region. Thus our ages can be taken as upper limits to the age of the most recent major episodes of star formation along the line of sight.

While the starburst ages that we list on Table 2 represent the best fit to the observed spectrum, there is a range of ages in each case that produces a reasonable fit. Figure 4 shows the spectrum from region B8 with three different solutions superposed: The youngest that still looks reasonable (top), the best fit (middle), and the oldest that still looks reasonable (bottom). In each case, the relative contribution of the old population was increased or decreased to give the best fit. The difference in χ^2 statistic between the middle and top or middle and bottom fits is 15%. We take these limits to be an estimate of the error in the determination of age so that, for this particular case, the starburst age would

be $114 (+67; -42)$ M yr. In general, a reasonable estimate of the error for the starburst age determined in each case is $\sim 50\%$.

As mentioned in §3.1, absorption lines in many regions are contaminated by emission lines coming from the extended ionized gas. In modeling these regions, we excluded those Balmer lines that were obviously contaminated by emission from the H^2 jets.

Notice that in some of the spectra (e.g., G2 in Fig. 3), the observed data are slightly depressed with respect to the models in the region between 4600 Å and 4800 Å. We previously found this problem in the spectrum of the companion to PG 1700+518 (Catalano & Stockton 1997) and attributed it there to an artifact of the subtraction of the QSO scattered light. However, some of the spectra of 3C 48 show this problem even when no QSO light was subtracted. We find no evidence for a correlation of this effect with the age of the starburst. Fritze-von Alvensleben & Gerhard (1994) seem to have run into the same problem when they use their own models to fit a spectrum of NGC 7252 (see their Fig. 1). This problem is also evident in the spectrum of G 515 in Liu & Green 1996. Neither of these groups discusses the discrepancy.

3.2.2. Mapping Stellar Populations

Figure 1c shows a map of the host galaxy with the starburst ages we determine from spectra. Figure 3 shows a characteristic spectrum of each of the regions described below. In column (3) of Table 2 we list the ages of the young stellar component for each region analyzed. In columns (4) and (5) we give, respectively, the mass and light (at 4500 Å, rest wavelength) contribution of the starburst to the observed spectrum.

We start with the long extension to the north-west of the quasar which is very likely a tidal tail, as we shall see. As we mentioned in the previous section, the stellar populations in most of this tail appear to have no younger component. Panel C8 of Fig. 3 shows one such spectrum with a fit to a 10 Gyr-old population with an exponentially decreasing star formation rate with an e-folding time of 5 Gyr.

Even though most of the extension is made up by old populations, there is one small starburst region covered by our slit positions G and A. This starburst has an age ~ 33 M yr and is about 4° west and 8° north of the quasar nucleus, where A7 and G8 intersect (see Fig. 1a,c). A faint clump at the same position is clearly seen on our U^0 ground-based image (Fig. 2d).

The U^0 image also shows two additional larger bright regions north of the quasar

nucleus. The eastern region corresponds to a strong emission region clearly seen in the [O III] λ 4960 image shown in Fig. 2f. The western region (covered by C 6 and adjacent regions in Fig. 1), on the other hand, is much fainter in both the narrow-band and broad-band images than in the U⁰ image. This region contains starbursts of ages \sim 9 M yr, and the F555W HST image suggests that it is formed of several smaller clumps.

We also find starburst ages \sim 9 M yr in the regions directly north (C 3, C 4) and southwest (G 3) of the quasar. These are seen in the U⁰ image as relatively high surface brightness areas. The area corresponding to G 3 has a knotty structure, which is not obvious in the longer wavelength images.

We have tried taking the ratio of our U⁰ image to our R⁰ image (Fig. 2e). Both of these images should be strongly dominated by continuum radiation; however, the physical interpretation of this ratio is not straightforward for two reasons: (1) while the U⁰ image should relatively emphasize regions that have young stars, it may also be enhanced by strong nebular thermal emission from emission regions, and (2) as our modeling of the stellar populations shows, the ratio of young and old stellar populations in the R⁰ image is highly variable. Nevertheless, a striking feature of the ratio image is the apparent ridge of strong UV radiation along the leading edge of the NW tail. This is apparently a complex of emission regions and young stars, including both the brightest emission region seen in the [O III] λ 4960 images and the A 7/G 8 star-forming region mentioned above.

On the west side of the nucleus (along Slit G) we find that there is no recent star formation in the northern half of the slit other than the star-forming clumps mentioned above. The southern part of the host galaxy seems to be dominated by relatively older starbursts (generally $>$ 100 M yr) with a range of ages between 16 and 114 M yr.

Finally, the youngest populations we observe in the host galaxy are found in the regions coincident with the two brightest features in the U⁰ image (see inset in Fig. 2d): (1) a region \sim 2⁰⁰ SE of the quasar, covered by A 3 and B 5, and (2) a region \sim 1⁰⁰ NE of the quasar, surrounded by B 3 and C 2, which will be discussed in more detail in §4.2. We find starburst ages as young as 4 M yr in these regions. Such young ages are comparable to starburst timescales and it is virtually impossible to distinguish between continuous star formation and instantaneous bursts, so the young ages we derive simply indicate that there is ongoing star formation.

3.3. Emission

3.3.1. Emission in the Quasar Nucleus

Thuan, Oke, & Bergeron (1979) noticed that the broad permitted emission lines in the spectrum of 3C 48 had a systematically higher redshift, by about 600 km s^{-1} , than did the forbidden lines. Boroson & Oke (1982) confirmed this qualitative result but found a lower velocity difference of $330 \pm 78 \text{ km s}^{-1}$. Gelderman & Whittle (1994) mentioned that the redshift of the forbidden lines is difficult to measure because they "have approximately flat tops."

Our spectrum of the quasar nucleus in the region around H β and [O III] $\lambda\lambda$ 4959,5007 is shown Fig. 5. The [O III] lines clearly have double peaks. By deconvolving the lines into best-fit Gaussian components, we find that the narrower, higher velocity component has a mean redshift $z = 0.36942$, with a Gaussian width $\sigma = 400 \text{ km s}^{-1}$, while the broader, lower-velocity component has a mean redshift $z = 0.36681$, with $\sigma = 700 \text{ km s}^{-1}$. These redshifts correspond to a velocity difference of $563 \pm 40 \text{ km s}^{-1}$. The redshift of the broad H β line is $z = 0.36935$, in good agreement with the higher-redshift [O III] line. Thus the anomalous feature is the broad, lower-velocity [O III] line.

What is the nature of this blue-shifted component? First, it is highly luminous: the luminosity in the [O III] λ 5007 line alone is $\sim 5 \times 10^{43} \text{ erg s}^{-1}$, over 3 times the luminosity of the same line in the "standard" narrow-line region. Second, it does show some spatially-resolved velocity structure, though only over a region of about $0.05''$. We first noticed this velocity gradient in our reduced long-slit spectrum, but it is very difficult to display because of the strong variation of the underlying quasar continuum in the direction perpendicular to the slit. Figure 6 shows the result of a PLUCY (Hook et al. 1994) deconvolution of the 2-dimensional spectrum, followed by a reweighting of the image perpendicular to the slit to even out the dynamic range in the resolved emission. The steep velocity gradient is clearly visible in the blueshifted component of both of the [O III] lines.

As we were completing this paper, an important new study by Chatzichristou, Vanderriest, & Jaffe (1999) appeared, in which the spatial and velocity structure of the emission lines in the inner region of 3C 48 were mapped with a fiber integral-field spectroscopic unit. They also observed the double-peaked narrow-line emission in the quasar spectrum, and their decomposition of the profile gave a radial velocity difference of $586 \pm 15 \text{ km s}^{-1}$, with which our value of $563 \pm 40 \text{ km s}^{-1}$ is in good agreement. Our results are in general agreement on most other points for which the two datasets overlap, except that Chatzichristou et al. find the luminous broad blueshifted component to have no resolved velocity structure, whereas we find it to have a strong velocity gradient over the central $0.05''$ region.

3.3.2. Extended Emission

We have a total of 6 slit positions useful for studying the extended emission, which are shown in Fig. 7, superposed on our narrow-band $[\text{O III}]$ image. Images of the two-dimensional spectra are shown in Fig. 8. We have fitted Gaussian profiles to the $[\text{O III}]$ 5007 lines (and to the $[\text{O II}]$ 3726,3729 lines in our higher-dispersion spectra from slits E and F) in order to measure the velocity field of the extended emission. At some positions, we had to use up to 3 components in order to get a satisfactory fit to the observed profile. The results are shown in Fig. 9, where the velocities, fluxes, and widths of the lines are indicated at each position. We also plot the velocities of the stellar component for slit positions A, B, C, and G. While there is generally at least rough agreement between the velocities of the stars and at least one component of the emission-line gas, there are significant differences in detail. Little, if any, of the emission can be due to an undisturbed in situ interstellar medium. The total velocity range of the emission is over 1200 km s^{-1} , and the FWHM of the emission reaches up to 2000 km s^{-1} .

The morphology of the extended emission, as seen in our deep ground-based $[\text{O III}]$ 5007 image (Fig. 2f) and the HST W FPC2 linear ramp filter image in the same emission line (Fig. 2i), consists of several discrete emission regions having characteristic sizes ranging from a few hundred pc to 1 kpc, connected by a web of lower-surface-brightness emission. Some of the emission regions lie outside the host galaxy, as defined by the deep continuum images. The HST image shows an apparent bright object about $0^{\circ}8$ S of the quasar, which has no counterpart on the HST continuum images. Kihakos et al. (1999) have referred to this object as an H II region. Its absence on the HST continuum images would indicate an $[\text{O III}]$ 5007 equivalent width $> 4000 \text{ \AA}$. An equivalent width this large is not impossible: if the intensity ratio of $[\text{O III}]$ 5007 to H β is 10, as is common in extended emission regions around QSOs, the equivalent width of H β would be about a factor of 3 below that which would be expected from the nebular thermal continuum alone for a temperature of 15000 K. However, we estimate that the object's absence on the HST PC F555W image requires that the flux of $[\text{O II}]$ 3727 be $< 4\%$ that of $[\text{O III}]$ 5007, rather than the more typical 20%. Finally, we have carried out a careful deconvolution of our ground-based $[\text{O III}]$ image, which has an original FWHM of $0^{\circ}74$ for stellar profiles. On our deconvolved image, we could easily have seen any object as bright as the emission region $2^{\circ}5$ east of the quasar, which appears almost 10 times fainter than the apparent object $0^{\circ}8$ south of the quasar on the HST $[\text{O III}]$ image, but there is no feature present at this location on our deconvolved image. While the W FPC2 Instrument Handbook does not mention the presence of nearly in-focus ghost images, these doubts about the reality of the feature prompted us to check with Matthew McMaster, a data analyst at ST ScI specializing in W FPC2 instrument anomalies and reduction of linear ramp filter data. He examined a

calibration image of a star taken with the same filter and centered on nearly the same wavelength, and he found a similar feature at exactly the same position in relation to the star, concluding that the apparent object seen near 3C 48 is an artifact.

The resolution of the $[\text{O II}] \lambda\lambda 3726, 3729$ doublet in the brighter regions of the extended emission is of special interest, since electron densities can be determined from the intensity ratio (e.g., Osterbrock 1989). For the bright pair of regions centered $4''$ N of the quasar (see Fig. 2i), we find a ratio $I(3729)/I(3726) = 1.25 \pm 0.05$, corresponding to an electron density of 150 cm^{-3} , assuming an electron temperature $T_e = 10^4 \text{ K}$. This density is sufficiently high that it is unlikely that the emitting gas, at its location some 20 kpc projected distance from the quasar, is in hydrostatic pressure equilibrium with the surrounding medium. Instead, it is probably either confined gravitationally (if, for example, the gas is in a dark-matter dominated dwarf galaxy) or compressed by shocks due to collisions of gas clouds during the interaction. This latter process seems to be the more likely one, at least for the string of emission and star-forming regions along the leading edge of the NW tail of 3C 48.

4. Discussion

4.1. Evidence for a Merger

Our modeling of the stellar populations in the faint tail-like structure extending to the NW of the quasar indicates that this extension is made up mostly of old stars. The predominance of old stellar populations in a feature that clearly has a dynamical timescale much shorter than the age of the stars that comprise it points strongly to a tidal origin. (The possibility that the apparent old population is the result of a truncated IMF rather than actual old stars can be discounted since we observe unambiguously high mass stars in some clumps within the tail and elsewhere in the main body of the host.) There can be little doubt that the feature is indeed a tidal tail. If this tail has an inclination angle i between 30° and 60° with respect to the plane of the sky, the dynamical age of the feature is between 100 and 300 Myr. Since the oldest starburst ages we find in the host galaxy are 114 Myr, the dynamical age of the tail indicates that the starbursts were induced after the initial encounter of the interacting galaxies.

If the host galaxy of 3C 48 has undergone strong gravitational interaction with a second object, and both objects originally possessed cold stellar disks, one might expect to observe also counter-tidal features such as a second tidal tail. Boyce, Disney & Bleaken (1999) published the archival HST F555W image of 3C 48 and identified a second tidal tail

\stretching $8^{\circ}5$ to the south-east of the quasar". We see a hint of a \tail" south of the nucleus and extending towards the south-east in both the HST images and our R^0 image, but it is only about 6° long. The object that Boyce et al. seem to consider the SE end of the \tail" is a background galaxy at redshift $z = 0.8112$ (object 4 in Table 3). When this object is removed, the case for this tidal tail becomes considerably less compelling.

Another possible second tidal tail is the feature starting SE of the nucleus, but arching from the SE towards the SW. The broad-band optical ground-based images show a relatively bright feature extending 3° SE of the nucleus and the HST images show peculiar structure around the same area. This could be the tidal tail with clumps of star formation (see below) of the merging companion. Typically, double tails in merging systems appear to curve in the sense that they are roughly rotationally symmetric. If this SE extension is a tidal tail, the two tails would, instead, present more of a \gull-wing" appearance. While this is not the usual case, a combination of disks inclined to the plane of the mutual orbit and projection effects can lead to precisely such a configuration. The best-known example is \The Antennae" (NGC 4038/9; Whitmore & Schweitzer 1995 and references therein) whose configuration has been reproduced in numerical simulations (Barnes 1988; Toomre & Toomre 1972).

Our kinematic results clearly indicate that the NW tidal tail has approaching velocities with respect to the main body of the galaxy. On the other hand, we find some evidence that the south extension (s) has receding velocities. Whether the 3° SE extension is a tidal tail and the system has an Antennae-like configuration, or the longer extension mentioned by Boyce et al. (1999) is the tidal tail forming a more typical merging configuration, the observed velocities are qualitatively in agreement with what we would expect from theoretical models (Toomre & Toomre 1972). However, there is much uncertainty in the interpretation of these southern features, and at this stage we cannot conclusively decide which, if any, of these features is a real tidal tail.

Our spectroscopy confirms that the clumps in the NW tidal tail observed on HST images (Kihakos et al. 1999) are regions of star formation, with ages < 33 Myr. Similar clumps have been observed in a number of strongly interacting or merging systems such as NGC 3628 (Chromey et al. 1998), IRAS 19254-7245 (Mirabel, Lutz & Maza 1991), Arp 105 (Duc & Mirabel 1994) and NGC 7252 (Schweizer & Seitzer 1998). Small star forming clumps in the tidal tails of merging systems are also predicted by numerical simulations (e.g., Elmegreen, Kaufman & Thomasson 1993; Mihos & Hernquist 1996).

The observational evidence seems to indicate that 3C 48 is a major merger according to the definition of Mihos & Hernquist (1994, 1996), that is, a merger of two gas-rich galaxies of roughly comparable size. In addition, at least one of the galaxies probably had

a significant bulge component. In the absence of a bulge, merging galaxies are predicted to undergo early dissipation, producing central starbursts in the disks shortly after the initial encounter, when the galaxies are still widely separated, and leaving little gas to form stars at the time of the merger (Mihos & Hernquist 1996).

In the case of 3C 48, however, we observe that there are strong starbursts still going on while the galaxies are close to the final stages of merging. The detection of large amounts of molecular gas in 3C 48 (Scoville et al. 1993; Wink et al. 1997), along with the very young ages for starbursts that we observe (~ 4 Myr), indicates that high rates of star formation are still present in the inner regions. Merging disk/bulge/halo galaxies have much weaker initial encounter starbursts, so that most of the gas is conserved until the final merger and the rapid collapse of this gas drives a tremendous starburst in the center of the merging system.

The importance of the presence of a massive bulge in preserving gas for star formation at the time of the final merger depends on rather uncertain assumptions regarding the star-formation law. However, there is little disagreement that an interaction involving a disk that is marginally stable against bar formation will lead to enhanced star formation at the time of the initial passage. The fact that all of the starbursts we observe were produced after the tidal tail was first launched strongly suggests that the presence of a bulge was important in the case of 3C 48.

4.2. The Effect of the Radio Jet

As mentioned in x1, 3C 48 is a compact steep-spectrum radio source. The bright radio structure extends $\sim 0.5''$ and takes the form of a one-sided jet extending approximately to the N, but with considerable distortion and local irregularities (Simon et al. 1990; Wilkinson et al. 1991). Lower-surface-brightness emission extends in a fan to the E side of this jet and continues to the NE out to a distance of $\sim 1''$ from the nucleus. The structure of this radio emission indicates interaction with a dense gaseous medium (Wilkinson et al. 1991). Is there any evidence in the optical observations for such an interaction?

We see spatially resolved velocity structure in the strong blueshifted emission component near the nucleus, and we find weaker broad, high-velocity emission at greater distances. These high velocities, ranging from ~ 500 km s $^{-1}$ with respect to the systemic velocity to over twice that, cannot plausibly be due to gravitational dynamics. Instead, they very likely reflect the interaction of the radio jet with the ambient medium.

As mentioned in x3.2, some of the youngest stellar populations are found just NE of the

quasar. It was in this region that Stockton & Ridgway (1991) discovered what looked like a secondary nucleus 1^0 from the quasar nucleus, which they called 3C 48A. Figure 2g and h show WFPC2 PC images of 3C 48 from the HST archive, which confirm the object found in the ground-based imaging and show much intriguing structural detail. While it is still possible that this may be, in fact, the distorted nuclear regions of the companion galaxy in the final stages of merger, it now seems more likely that it, too, is related to the interaction of the radio jet with the dense surrounding medium, as suggested by Chatzichristou et al. (1999).

The WFPC2 PC images (Fig. 2g,h) show an almost circular edge brightening effect around 3C 48A, which Kihakos et al. 1999 suggest is an image ghost artifact. After careful inspection, we believe it to be a real feature, especially since it perfectly surrounds the peak seen in both the ground-based and HST imaging. The VLBI map of 3C 48 (Wilkinson et al. 1991) shows diffuse radio emission extending into this region. Together with the spectroscopic evidence, the radio morphology suggests that this edge-brightening effect may be the remains of a bubble, where the radio jet had recently, but temporarily, broken through the dense gas in the inner region. We believe that this is not an active bubble at present because (1) the present jet appears to be directed along a more northerly direction, and (2) the shell-like structure is not apparent in the emission-line image, indicating that it probably comprises stars, which may have been formed as shocks compressed the gas at the boundaries of the bubble.

From the weakness of the core component in 3C 48, Wilkinson et al. (1991) argue that the radio jet is truly one sided, i.e., we are not missing an oppositely directed jet simply because of Doppler boosting. Our spectroscopy tends to confirm this view: we see widespread high-velocity gas with blueshifts relative to the systemic velocity, but not with redshifts.

5. Summary and Conclusions

In summary,

We have measured redshifts from stellar absorption features in 32 regions of the host galaxy. The average redshift in the central region of the host is close to $z = 0.3700$, and there are relatively small variations ($\sim 50 \text{ km s}^{-1}$) in the main body of the galaxy. The large faint feature extending NW of the quasar is clearly blueshifted with respect to the main body of the host galaxy by as much as 300 km s^{-1} . Some regions in the SE of the galaxy are redshifted, suggesting that the system is rotating about an axis

oriented roughly NE | SW .

We have successfully modeled the stellar populations in the same 32 regions of the host galaxy of 3C 48. Spectra from most regions can be modeled by an old stellar component plus an instantaneous burst population, presumably the stellar component present in the galaxies prior to interaction plus a starburst produced as a result of the interaction. Spectra from the remaining regions are well fit by the old component alone.

The feature extending NW of the quasar is a tidal tail composed mostly of an old stellar component, with clumps of recent star formation, much like those observed in other merging systems. The estimated dynamical age of this feature (between 0.1 and 0.3 G yr) is much younger than the age of the dominating stellar population (10 G yr) and roughly equal to or older than the starburst ages we find anywhere on the host (~ 0.11 G yr). Thus the starbursts occurred after the tidal tail was initially launched. This delay of most of the star formation until close to the time of final merger indicates that at least one of the merging galaxies probably had a massive bulge capable of stabilizing the gas in the inner disk.

We find very young stellar populations in the central regions of the host galaxy, with the youngest populations (~ 4 M yr) in a region $\sim 1^{\circ}$ NE of the quasar and in a region $\sim 2^{\circ}$ SE of the quasar. The youngest ages we find (< 10 M yr) indicate ongoing star formation.

The large amounts of observed CO (Scoville et al. 1993; Wink et al. 1997) along with the very large fractions of gas already used up to form stars in the starburst regions we observe indicate that 3C 48 may be near the peak of its starburst activity.

The extended emission is distributed mostly in several discrete regions. Most of this gas falls in one of two distinct velocity regimes: either (1) within ~ 200 km s⁻¹ of the systemic velocity, or (2) blueshifted with respect to the systemic velocity by ~ 500 km s⁻¹. Densities in at least the brighter clumps of extended emission are ~ 150 e cm⁻³, indicating probable compression by shocks resulting from the interaction. The presence of at least one region of recent star formation in the tail indicates that some of these clumps reach sufficient densities to become self-gravitating.

Extremely luminous high-velocity emission close to the quasar nucleus and extended emission with high velocities and large velocity widths, together with the convoluted shape of the VLBI radio jet, indicate a strong interaction between the radio jet and the ambient gas. The luminosity peak $\sim 1^{\circ}$ NE of the quasar and the edge-brightening

around this region seen in the HST images may be a relic of a previous, but still quite recent, interaction between the radio plasma and the ambient material.

From these results, we can outline a tentative evolutionary history for the host galaxy of 3C 48. Two gas-rich galaxies of comparable mass, at least one of which has a massive bulge, interact strongly enough for tidal friction to have a significant influence on their mutual orbit. The orbit is prograde with respect to the stellar disk of at least one of the galaxies, and, at their first close passage, a tidal tail is produced from this disk. Little star formation occurs at this point, but the tail does include some gas which will later form small star-forming regions, particularly along the leading edge of the tail. Most of star formation is delayed by a few hundreds of Myrs until the final stages of merger, when gas flows into the center also trigger the quasar. A one-sided radio jet is produced, which interacts strongly with the dense gas that has accumulated near the center, producing a bubble of shocked gas to the NE of the quasar. The shocked gas at the boundary of this bubble forms stars; shortly afterwards, the jet is deflected along a more northerly direction.

Information on stellar populations in host galaxies and close companions to QSOs can potentially give us a substantial lever in attempting to sort out the nature and time scales of various phenomena associated with the initiation and evolution of QSO activity. Numerical simulations suggest that the peak of starburst activity for mergers occurs at roughly the same time as a major gas inflow towards the center of the galaxy, so the time elapsed since the peak of the central starburst may be approximately coincident with the QSO age. Thus, by determining starburst ages in these objects we may be able to place them on an age sequence, and this in turn may help clarify the relationship between ULIGs and QSOs.

In particular, our results are suggestive of a connection between 3C 48 and the ULIG population. We have shown that 3C 48 is likely to be near the peak of the starburst activity, which would place it near the beginning of the age sequence mentioned above. We have also presented evidence that 3C 48 is in the final stages of a merger; ULIGs are found preferentially in the final merging phase (Surace et al. 1998; Mihos 1999). Further, 3C 48 occupies a place in the FIR diagram close to that of ULIGs (Neugebauer et al. 1986; Stockton & Ridgway 1991), and Haas et al. 1998 find that the FIR emission of 3C 48 is unambiguously dominated by thermal emission. Indeed the mass and dominant temperature of dust in 3C 48 appears to be very similar to that of ULIGs (Klaas et al. 1997; Haas et al. 1998). In short, if the evolutionary sequence proposed by Sanders et al. (1988) is correct, 3C 48 seems to be viewed right after the optical QSO becomes visible.

While this scenario may seem plausible, there are clearly a number of worries. To what extent is it legitimate to use a star-formation age measured several kpc from the

nucleus as a proxy for that in the nucleus itself, which is the age that we might expect to be most closely correlated with that of the QSO activity? Given that we are not sure what angular-momentum transfer mechanisms operate to bring the gas from the 100-pc-scale of the central starburst to the sub-pc scale of the QSO accretion disk, is our assumption that the starburst peak and the triggering of the QSO activity are more-or-less contemporaneous valid?

The picture also becomes more complex when one tries to make sense of recent related observations. Tran et al. 1999 concluded that QSOs are likely to be found only in host galaxies with a dominant stellar population older than 300 Myr. Apparently, their reasoning is based on the observation that ULIGs have starbursts with mean ages of \sim 300 Myr, and the belief that the active nucleus only becomes visible at a later stage. 3C 48 is a clear counterexample to this view. There clearly must be a dispersion, and quite likely a rather broad one, in the properties of ULIGs that govern the time it takes for dust to be cleared from the inner regions. Even more important may be the viewing angle. For 3C 48, there is almost certainly a range of lines of sight for which the quasar is hidden and the object would be classified solely as an ULIG.

In a study of off-nuclear optical spectroscopy of 19 QSO host galaxies, Kukula et al. 1997 found much older dominant stellar populations in the hosts, with ages ranging from \sim 2 Gyr to \sim 11 Gyr. While there certainly do seem to be QSOs for which the host-galaxy spectrum is dominated by old stars, our detailed study of 3C 48 does inject a note of caution regarding such determinations, particularly those based on a single slit position in the outskirts of the host galaxy. If we were to confine our interpretation of the stellar population of 3C 48 to an integrated spectrum from points $> 6''$ from the quasar, we would have found only an old population. However, it is clear that our selection of QSOs with FIR colors similar to those of ULIGs has strongly biased our results; in fact, none of the host galaxies or strongly interacting companions in this sample that we have yet observed (e.g., PG 1700+518: Canalizo & Stockton 1997; Stockton, Canalizo & Ciose 1998; Mrk 231, IR 0759+651, Mrk 1014: Canalizo & Stockton 2000) show dominant populations as old as the youngest of those observed by Kukula et al. 1997.

On a more speculative note, there may be a correlation between the morphology of the merging galaxies, the star-formation properties, and the QSO properties. If the models of Mihos & Hernquist (1996) are at least qualitatively correct, mergers involving disk galaxies of nearly equal mass, but with insignificant bulges, will have a rather broad peak of star formation in which they use up most of their available gas near the time of first passage, leaving little for further star formation at the time of final merger. Similar mergers involving pairs with substantial, centrally concentrated bulges have only a small amount of

star formation prior to their final merger, when most of the star formation occurs in quite a sharp peak. Thus one expects the most luminous starbursts to be in mergers involving gas-rich galaxies with massive bulges. Comparison of Monte-Carlo simulations of mergers with images of a sample of ULIGS does indicate that most of the latter are in the late stages of merger, consistent with stability of their inner disks over the early phases of the interaction (Mihos 1999).

While bulges may be important in determining the timing and the rate of star formation during an interaction, they may also have some bearing on the nature and strength of the nuclear activity. The recent demonstration of an apparent correlation between bulge mass and black-hole mass (Magorrian et al. 1998) indicates that those mergers for which gas flows into the center are delayed by the presence of stabilizing bulges and that those with the highest intrinsic flow rates may also involve the most massive black holes. If QSO luminosities are statistically correlated with the Eddington limits on their black-hole accretion rates, then these sorts of mergers are likely to produce the most luminous QSOs. While there are many qualifications to this scenario (e.g., current N-body simulations fall several orders of magnitude short of being able to follow the gas to the scale of the accretion disk; feedback from stellar winds and supernova outflows on the infalling gas is not well treated), it does at least supply a motivation to be alert to possible differences between QSOs for which the star formation and nuclear activity occur while the objects are still distinctly separated, such as PG 1700+518 (Canalizo & Stockton 1997; Stockton et al. 1998) and those, like 3C 48, where the activity appears to peak close to the time of final merger.

We thank Bill Vacca, John Tonry, Dave Sanders, and Josh Barnes for helpful discussions, and Susan Ridgway for assisting in some of the observations. We also thank Richard Hook for supplying us with his CPLUCY routine and Matt McMaster for his detective work in confirming the spurious nature of the apparent object near 3C 48 in the HST [O III] image. We are grateful to the referee, Linda Dressel, for useful comments and suggestions. This research was partially supported by NSF under grant AST 95-29078.

A . Serendipitous Objects Around 3C 48

A number of objects in the field of 3C 48 fell on our various slit positions. We measured redshifts for those objects which could also be identified in the HST images. Table 3 lists these objects with their coordinates (J2000.0) as measured from the HST images, redshift, whether the redshift was determined from emission or absorption features, and the slit position ID (see x2).

Gehren et al. (1984) suggest that the object $12^{\text{h}} 00^{\text{m}}$ NW of the quasar nucleus may be a companion galaxy to 3C 48. This object falls on the edge of our slit position E. We see evidence for a faint emission line at the 2.5σ level, wide enough at this resolution to be $[\text{O II}] \lambda 3727$. If this were the case, the redshift of the object would be $z = 0.378$ ($v = 1800 \text{ km s}^{-1}$ with respect to our zero velocity point in the host galaxy). This object is not listed on Table 3.

Only one object in Table 3 has a redshift relatively close to that of 3C 48. This may indicate that 3C 48 is in a low density cluster (Yee & Green 1987), if in a cluster at all.

The background galaxy $6^{\text{h}} 00^{\text{m}}$ SE of 3C 48 (object 4) stresses the importance of obtaining spectroscopic redshifts to discriminate between objects associated with QSOs and close projections.

REFERENCES

- Bames, J. E. 1988, *ApJ*, 331, 699
 Boroson, T. A., & Oke, J. B. 1982, *Nature*, 296, 397
 Boroson, T. A., & Oke, J. B. 1984, *ApJ*, 281, 535
 Boyce, P. J., Disney, M. J., & Bleaken, D. G. 1999, *MNRAS*, 302, L39
 Bruzual, G., & Charlot, S. 1996, unpublished
 Canalizo, G., & Stockton, A. 2000, in preparation
 Canalizo, G., Stockton, A., & Roth, K. C. 1998, *AJ*, 115, 890
 Canalizo, G., & Stockton, A. 1997, *ApJ*, 480, L5
 Chatzichristou, E. T., Vanderriest, C., & Jaffe, W. 1999, *A&A*, 343, 407
 Chromey, F. R., Elmegreen, D. M., Mandell, A., & McDermott, J. 1998, *AJ*, 115, 2331
 Duc, P.-A., & Mirabel, I. F. 1994, *A&A*, 289, 83
 Elmegreen, B. G., Kaufman, M., & Thomasson, M. 1993, *ApJ*, 412, 90

- Fritze-von Alvensleben, U. & Gerhard, O. E. 1994, *A & A*, 285, 775
- Gelderman, R., & Whittle, M. 1994, *ApJS*, 91, 491
- Haas, M., Chini, R., Meisenheimer, K., Stickel, M., Lemke, D., Klaas, U., & Kreysa, E. 1998, *ApJ*, 503, L109
- Heckman, T. M., Gonzalez-Delgado, R., Leitherer, C., Meurer, G. R., Kollk, J., Wilson, A. S., Koratkar, A., & Kinney, A. 1997, *ApJ*, 482, 114
- Hook, R. N. 1998, private communication
- Hook, R. N., Lucy, L. B., Stockton, A., & Ridgway, S. E. 1994, *ST-ECF Newsl*, 21, 16
- Kirkhakov, S., Bahcall, J. N., Schneider, D. P., & Kristian, J. 1999, *ApJ*, 520, 67
- Klaas, U., Haas, M., Heinrichsen, I., Schutz, B. 1997, *A & A*, 325, L21
- Krist, J. 1993, in *ASP Conf. Ser.*, v. 52, *Astronomical Data Analysis Software and Systems II*, ed. R. J. Hanish, R. J. V. Brissenden, & J. Barnes (San Francisco: Astron. Soc. Pac.), p. 530
- Kristian, J. 1973, *ApJ*, 179, L61
- Leitherer, C., Vacca, W. D., Conti, P. S., Filippenko, A. V., Robert, C., Sargent, W. L. W. 1996, *ApJ*, 465, 717
- Liu, C. T. & Green, R. F. 1996, *ApJ*, 458, L63
- Magorrian, J., et al. 1998, *AJ*, 115, 2285
- Massey P., Strobel K., Barnes, J. V., & Anderson, E. 1988, *ApJ*, 328, 315
- Matthews, T. A., Bolton, J. G., Greenstein, J. L., Munch, G., & Sandage, A. R. 1961, *Sky and Telescope*, 21, 148
- Matthews, T. A., & Sandage, A. R. 1963, *ApJ*, 138, 30
- Mihos, J. C. 1999, *Ap&SS*, in press
- Mihos, J. C., & Hemquist L. 1996, *ApJ*, 464, 641
- Mihos, J. C., & Hemquist L. 1994, *ApJ*, 425, L13
- Mirabel, I. F., Lutz, D., & Maza, J. 1991, *A & A*, 243, 367
- Neugebauer, G., Miley, G. K., Soifer, B. T., & Clegg, P. E. 1986, *ApJ*, 308, 815
- Oke, J. B., et al. 1995, *PASP*, 107, 375
- Osterbrock, D. E. 1989, *Astrophysics of Gaseous Nebulae and Active Galactic Nuclei*, (Mill Valley, CA: University Science Books), p. 132

- Sanders, D . B ., Soifer, B . T ., Elias, J . H ., Madore, B . F ., Matthews, K ., Neugebauer, G ., & Scoville, N . Z . 1988, *ApJ*, 325, 74
- Sanders, D . B ., & Mirabel, I . F . 1996, *ARA & A*, 34, 749
- Schweizer, F . & Seitzer, P . 1998, *AJ*, 116, 2206
- Scoville, N . Z ., Padin, S ., Sanders, D . B ., Soifer, B . T ., & Yun, M . S . 1993, *ApJ*, 415, L75
- Simon, R . S ., Readhead, A . C . S ., Moutat, A . T ., Wilkinson, P . N ., Booth, R ., Allen, B ., & Burke, B . F . 1990, *ApJ*, 354, 140
- Stockton, A . 1999, in *Galaxy Interactions at Low and High Redshift*, IAU Symp. 186, eds. D . Sanders & J . Barnes (San Francisco: Astron. Soc. Pac.), p. 311
- Stockton, A ., Canalizo, G ., & Cløse, L . 1998, *ApJ*, 500, L121
- Stockton, A ., & Mackenty 1987, *ApJ*, 316, 584
- Stockton, A ., & Ridgway, S . E . 1991, *AJ*, 102, 488
- Surace, J . A ., Sanders, D . B ., Vacca, W . D ., Veilleux, S ., & Mazzarella, J . M . 1998, *ApJ*, 492, 116
- Thuan, T . X ., Oke, J . B ., Bergeron, J . 1979, *ApJ*, 230, 340
- Toomre, A ., & Toomre, J . 1972, *ApJ*, 178, 623
- Tran, H . D ., Brotherton, M . S ., Stanford, S . A ., van Breugel, W ., Dey, A ., Stem, D ., & Antonucci, R . 1999, *ApJ*, 516, 85
- Wampler, E . J ., Robinson, L . B ., Burbidge, E . M ., & Baldwin, J ., 1975, *ApJ*, 198, L49
- Whitmire, B . C ., & Schweitzer, F . 1995, *AJ*, 109, 960
- Wilkinson, P . N ., Tzioumis, A . K ., Benson, J . M ., Walker, R . C ., Simon, R . S ., & Kahn, F . D . 1991, *Nature*, 352, 313
- Wink, J . E ., Guilloteau, S ., & Wilson, T . L . 1997, *A & A*, 322, 427
- Yee, H . K . C ., & Green, R . F ., 1987, *ApJ*, 319, 28

Fig. 1. | Maps indicating slit positions, stellar radial velocities, and starburst ages of the host galaxy of 3C 48. The contour maps are of an image similar to that of Fig. 2a, and the contours are drawn at logarithmic steps. In all panels N is up and E to the left, and the tick marks are in arcseconds. (a) Region IDs: Slit positions A, B, C and G indicating the regions into which we have subdivided each slit for analysis. (b) Radial Velocity Map: Shading indicates radial velocity with respect to $z = 0.3700$ (close to the average redshift in the central regions of the host galaxy) measured from stellar absorption features. (c) Starburst Age Map: Shading indicates ages of instantaneous burst populations determined from our modeling (see text for details). Scalebar is logarithmic; three tick marks are drawn at 10, 50, and 100 Myr respectively. The hatched regions indicate the predominance of an old stellar population, i.e., regions in which the observed spectrum is well fit by the old stellar population model alone.

Fig. 2. | Ground-based and HST WFC2 images of 3C 48. In all cases, N is up and E to the left. In all insets, when present, show lower-contrast versions. Details of the observations are given in §2 of the text. (a) Image obtained with an interference filter centered at 6120 Å, with a FWHM of 960 Å, covering the mostly emission-line-free rest frame region 4120–4820 Å. This image has been deconvolved and had the quasar profile removed with CPLUCY (Hook 1998). The white cross indicates the position of the quasar. The image prior to CPLUCY processing is shown in (b) and a lower-contrast version of (a) is shown in (c). (d) Image in the rest-frame continuum near 2500 Å, also processed with CPLUCY. (e) Ratio of the U^0 image (d) to the R^0 image (a). Both images have been smoothed to the same resolution, and regions with a $S/N < 2$ in either image have been suppressed. (f) Image through a 30 Å FWHM filter centered on the redshifted [O III] 5007 emission line. (g–i) Archival images obtained with HST and WFC2 (filters as labeled; note that these images are enlarged by a factor of 2 relative to the other images). (g) and (h) were obtained with PC1 and (i) with WFC2 and a linear-ramp filter.

Fig. 3. | Characteristic spectra of different regions of the host galaxy of 3C 48. Each panel displays the observed data in rest frame (heavy line), an underlying old stellar population model (lower light line), a young instantaneous starburst model (upper light line), and the χ^2 fit of the sum of the two models to the data (dotted line). The old model is a 10 Gyr old stellar population with an exponentially decreasing star formation rate with an e-folding time of 5 Gyr. Each panel is labeled with the region ID it represents (cf. Fig. 1). The original data have been smoothed with Gaussian filters with $\sigma = 2 \text{ \AA}$. Emission lines seen in these spectra come from the extended-emission region of the quasar and not from the star-forming regions.

Fig. 4. | Estimating errors in age determination. The observed spectrum from region B8 (solid line) with three different solutions superposed (dotted line): The youngest that still looks reasonable (top), the best fit (middle), and the oldest that still looks reasonable (bottom). The ages of the young starbursts are 72, 114, and 181 Myr respectively. In each case, the relative contribution of the old population was increased or decreased to give the best fit. The difference in χ^2 statistic between the middle and top or middle and bottom fits is 15%. The flux-density scale refers to the middle spectrum; the upper and lower spectra have been displaced by arbitrary amounts.

Fig. 5. | Trace of the nuclear spectrum of 3C 48, showing the double peaks in the [O III] lines. The spectrum has been reduced to the rest frame using the redshift of the longward component, which closely matches the broad-line redshift. The redward side of the [O III] 5007 line is slightly affected by atmospheric B-band absorption; even more so is the Fe II 5018 emission, which appears as a small, displaced peak to the right of the [O III] 5007 line.

Fig. 6. | Deconvolved spectrum from slit A. This image was produced by first subtracting out as much of the nuclear continuum as possible without producing negative residuals, running a PLUCY deconvolution (Hook et al. 1994) with no point-source components, and dividing the result by an image smoothly varying as a function of slit coordinate and designed to reduce the large dynamic range in the emission component intensities. While this procedure produces negative artifacts near strong emission features and gives a distorted view of the strengths of the various emission components, it clearly shows the strong velocity gradient in the strong anomalous narrow-line region near the nucleus.

Fig. 7. | Slit positions superposed on the [O III] emission image. The inner region is shown at lower contrast in the main panel, and the inset shows most of the extended emission components at an intermediate contrast.

Fig. 8. | Two-dimensional spectral images, showing either the [O III] 4959;5007 or the [O II] 3726;3729 lines. Slit orientations are shown in Fig. 7. Note the broad, blue-shifted components, seen most obviously in slits B, C, and G.

Fig. 9. | Overview of the properties of the emission-line gas observed in each of six slits, and the relation of the gas velocities and stellar velocities along the lines of sight. The circles are centered on the velocity and position of each emission-line component detected, and their areas are proportional to the flux at that point. The horizontal lines are proportional to the Gaussian FWHM. The scale for each of these measures is given in the lower-left corner of each panel: the circle corresponds to 10^{16} erg cm^{-2} s^{-1} per 1-pixel row ($= 0.215$) in the spatial dimension, and the line corresponds to a FWHM of 400 km s^{-1} . The points with error bars give the stellar velocities for each slit. The horizontal bars on these points give velocity uncertainties, but the vertical bars give the spatial range over which the velocity is an average. The zero point of the spatial axis for Slit A is centered on the quasar; that for the other slits is referenced to the point closest to the quasar. The asterisk (*) in the diagram for Slit F indicates a region for which emission was observed, but multiple components and a large velocity dispersion made measurements of the $[\text{O II}]$ doublet impossible. This region roughly corresponds to that covered by Slit C for $-1 < y < 0$.

Table 1. Journal of Spectroscopic Observations

Slit ID	PA (deg)	Offset (arcsec)	Slit Width (arcsec)	Dispersion (\AA pixel^{-1})	UT Date
A	332.7	0.0	1.0	1.28	96 Oct 13
B	13.5	1.9 E	1.0	1.28	96 Oct 13
C	300.0	2.5 N	1.0	1.28	96 Oct 13
D	185.0	0.0	0.7	0.85	96 Oct 14
E	100.0	3.8 N	1.0	0.85	96 Nov 03
F	148.0	2.1 E	0.7	0.85	96 Nov 03
G	167.0	2.2 W	1.0	1.28	96 Nov 04

Table 2. Stellar Populations and Kinematics

Region ID	Velocity ^a (km s ⁻¹)		Age ^b (Myr)	% Mass ^c	% Light ^d	% QSO Contamination ^{d,e}
A 1	+179	18	50	3.6	42	15
A 2	+107	41	114	3.4	33	30
A 3	+46	20	4.8	0.6	41	63
A 4	86	120	9.1	2.9	63	61
A 5	148	102	9.1	1.6	47	34
A 6	261	50	8.7	0.6	25	17
A 7	212	78	14	1.5	45	0
A 8	147	94	old	0.0	0	0
B 1	2	92	8.3	1.3	47	34
B 2	+42	52	9.1	2.3	56	46
B 3	+20	16	4.4	1.6	63	59
B 4	2	25	6.3	15.2	94	63
B 5	+48	18	4.8	1.5	67	27
B 6	+28	20	102	11.4	63	16
B 7	30	30	102	7.4	51	6
B 8	33	51	114	11.0	60	0
C 1	+11	26	5.5	12.2	92	48
C 2	+17	33	5.5	1.0	48	42
C 3	+4	65	9.1	2.0	53	32
C 4	57	21	8.7	2.3	59	12
C 5	112	52	8.7	2.0	54	0
C 6	298	92	9.1	1.4	44	0
C 7	335	30	old	0.0	0	0
C 8	175	61	old	0.0	0	0
G 1	+103	74	35	5.1	54	0
G 2	+4	27	16	4.0	62	0
G 3	28	14	9.1	2.4	58	67
G 4	+66	44	old	0.0	0	82
G 5	129	60	old	0.0	0	78
G 6	287	30	9.1	1.3	41	0
G 7	325	98	old	0.0	0	0
G 8	194	30	33	7.0	64	0

^aRelative to a systemic redshift $z = 0.3700$ ^bError estimates for starburst age described on text. See also Fig. 4^cAssuming a Salpeter initial mass function

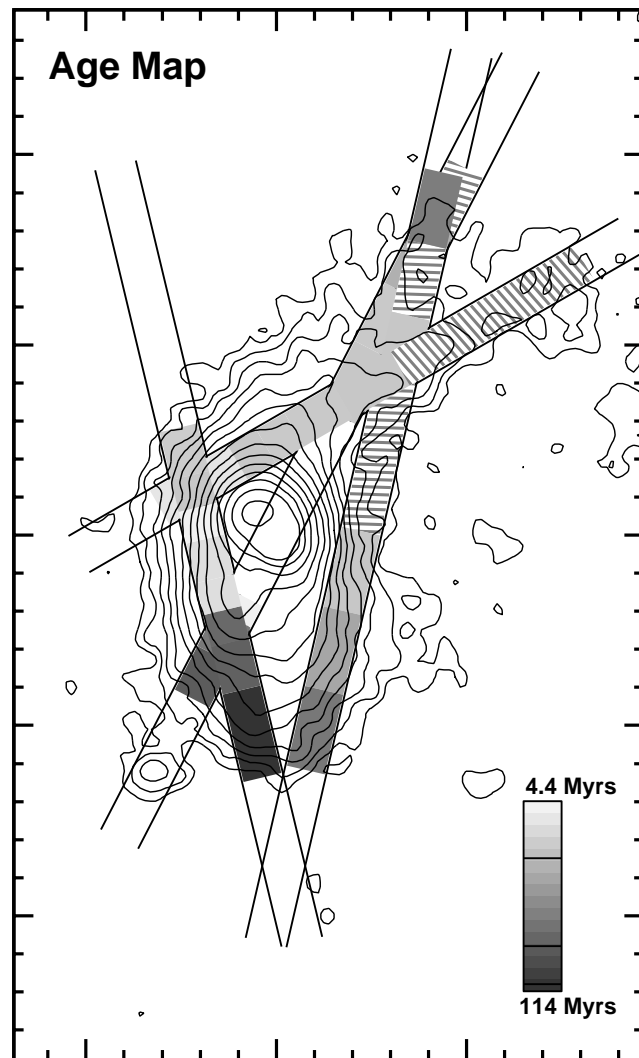
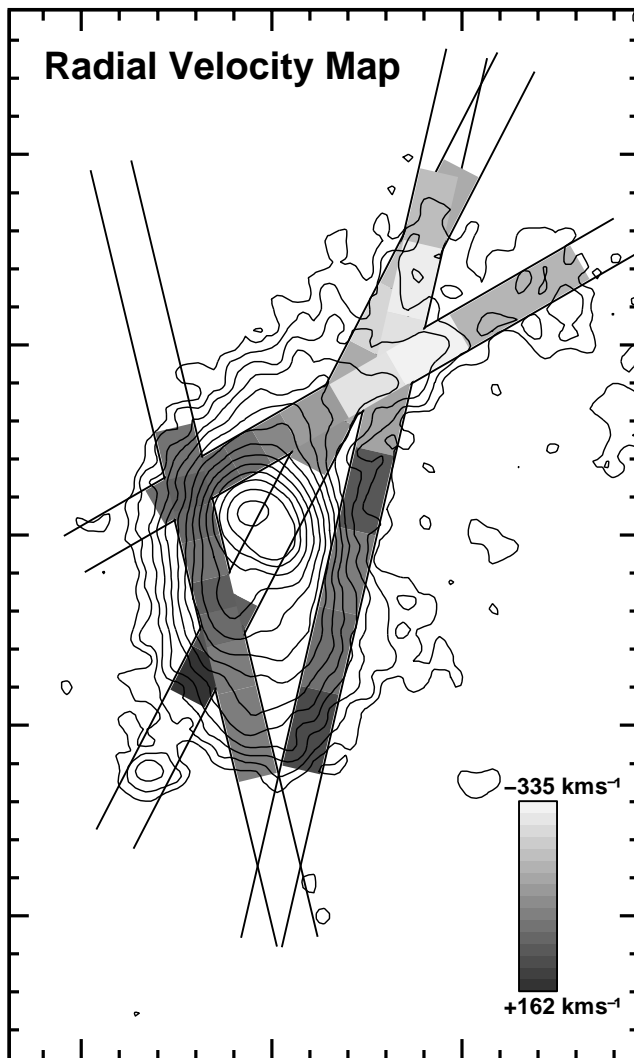
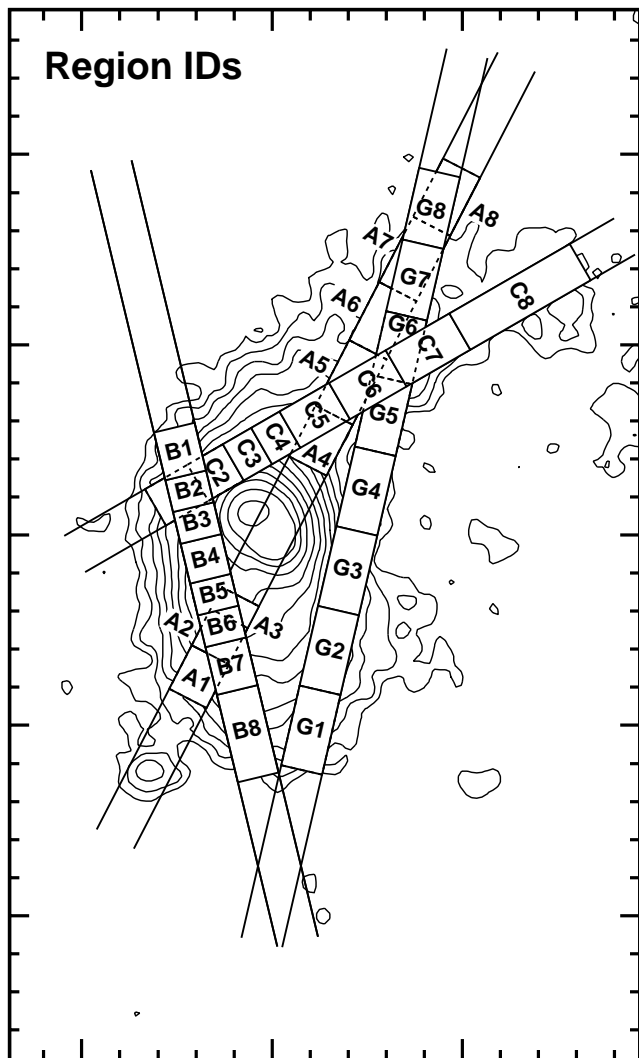
Table 3. Serendipitous Objects

ID	Coords (J2000)		Redshift ^a	Slit	Comments ^b
	RA	Dec		Position	
1	1 ^h 37 ^m 39 ^s .04	33 10 ^o 33 ['] .8	0.6722 e	A	interacting
2	1 37 42.33	33 09 09.0	0.7408 ea	A	disk
3	1 37 42.79	33 09 00.0	0.6730 ea	A	elliptical
4	1 37 41.54	33 09 29.0	0.8117 e	A	disk
5	1 37 40.67	33 08 56.8	2.169 e	B	BAL QSO ^c
6	1 37 42.15	33 09 22.9	?	F	continuum only
7	1 37 43.96	33 08 41.8	0.3560 e	F	disk
8	1 37 41.67	33 09 06.1	0.6430 a	G	elliptical
9	1 37 42.71	33 08 03.1	0.3279 ea	G	disk

^ae and a after redshift indicate whether redshift was measured from emission or absorption lines, respectively.

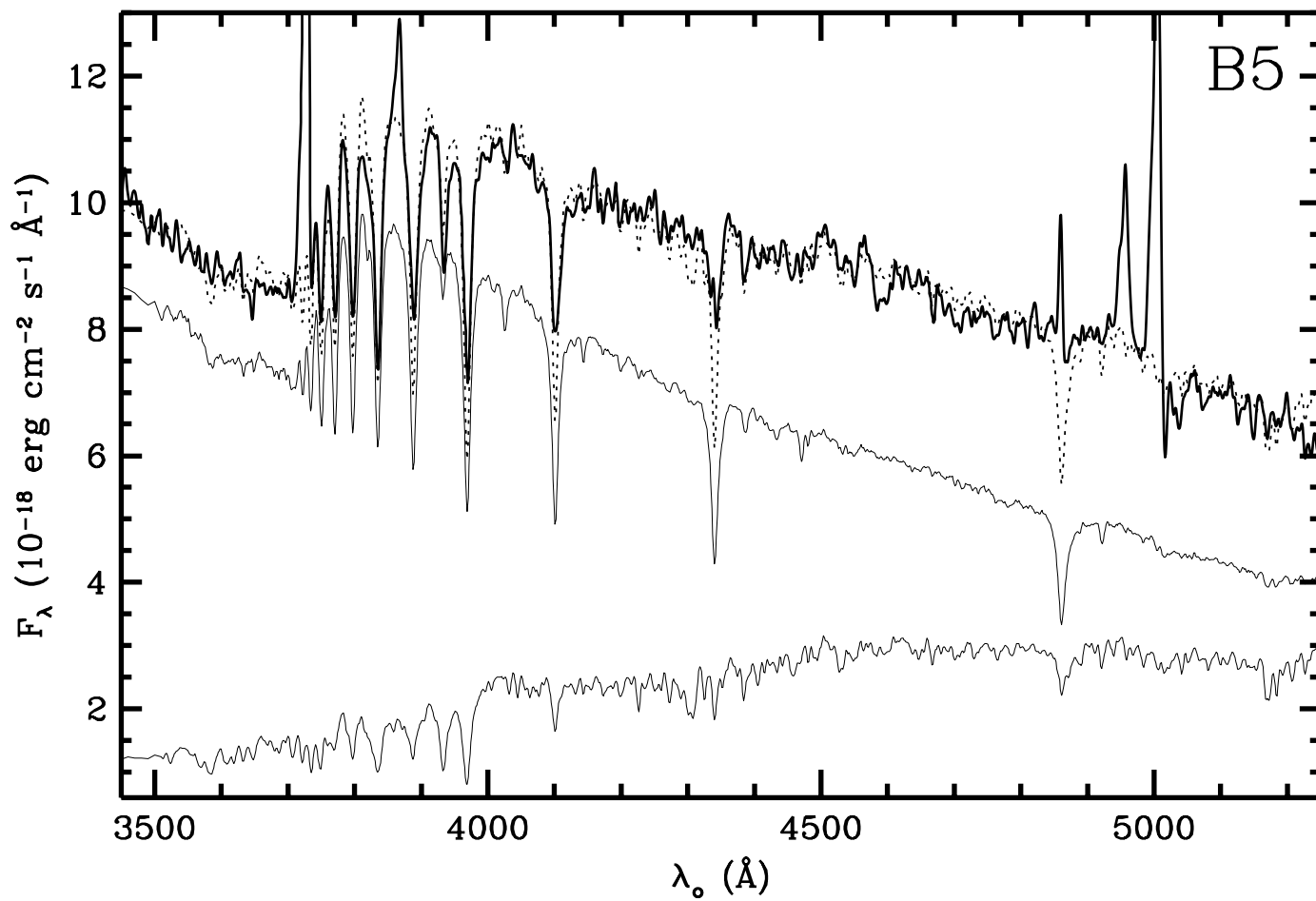
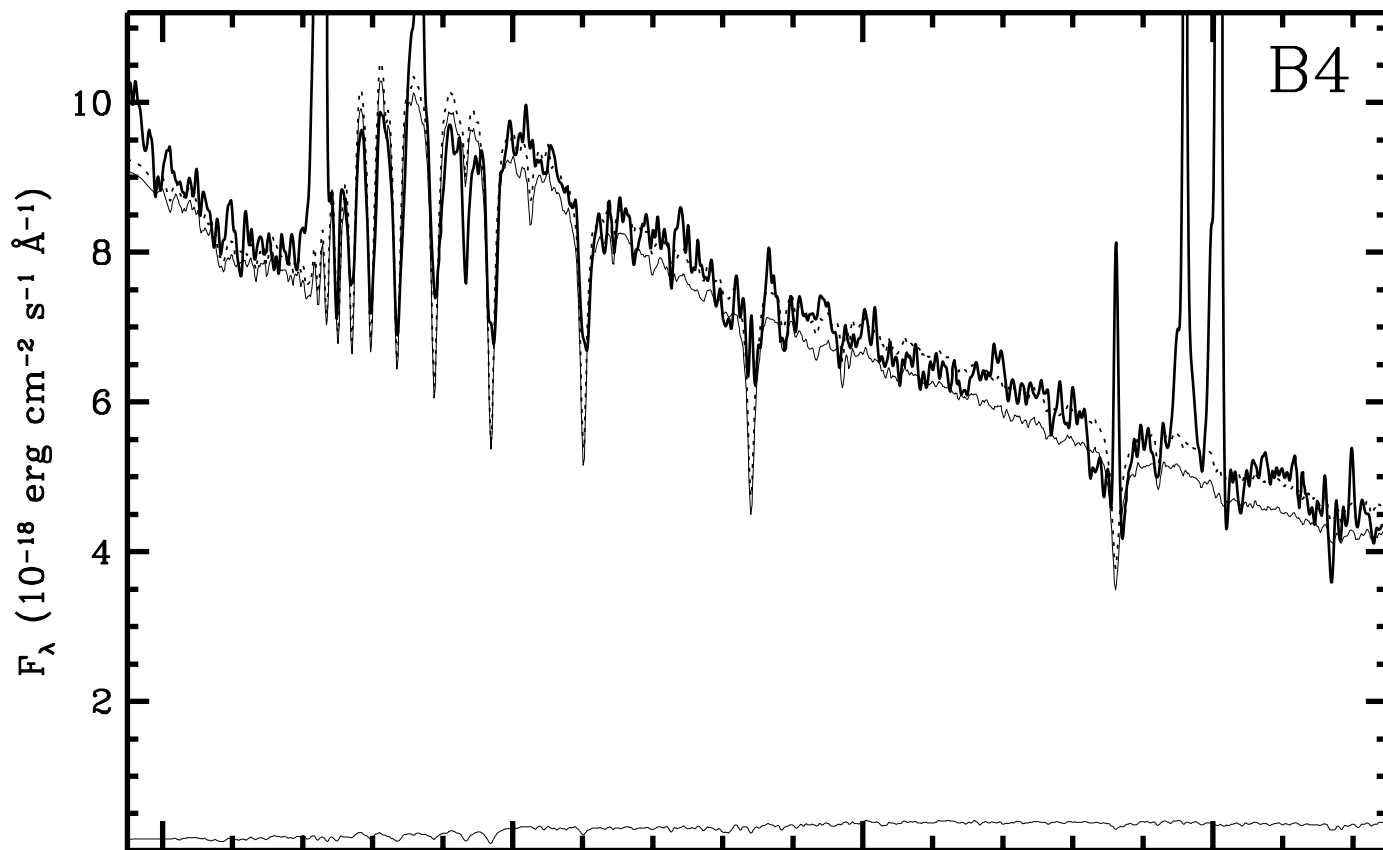
^bMorphologies are based on appearance on HST WFC2 images.

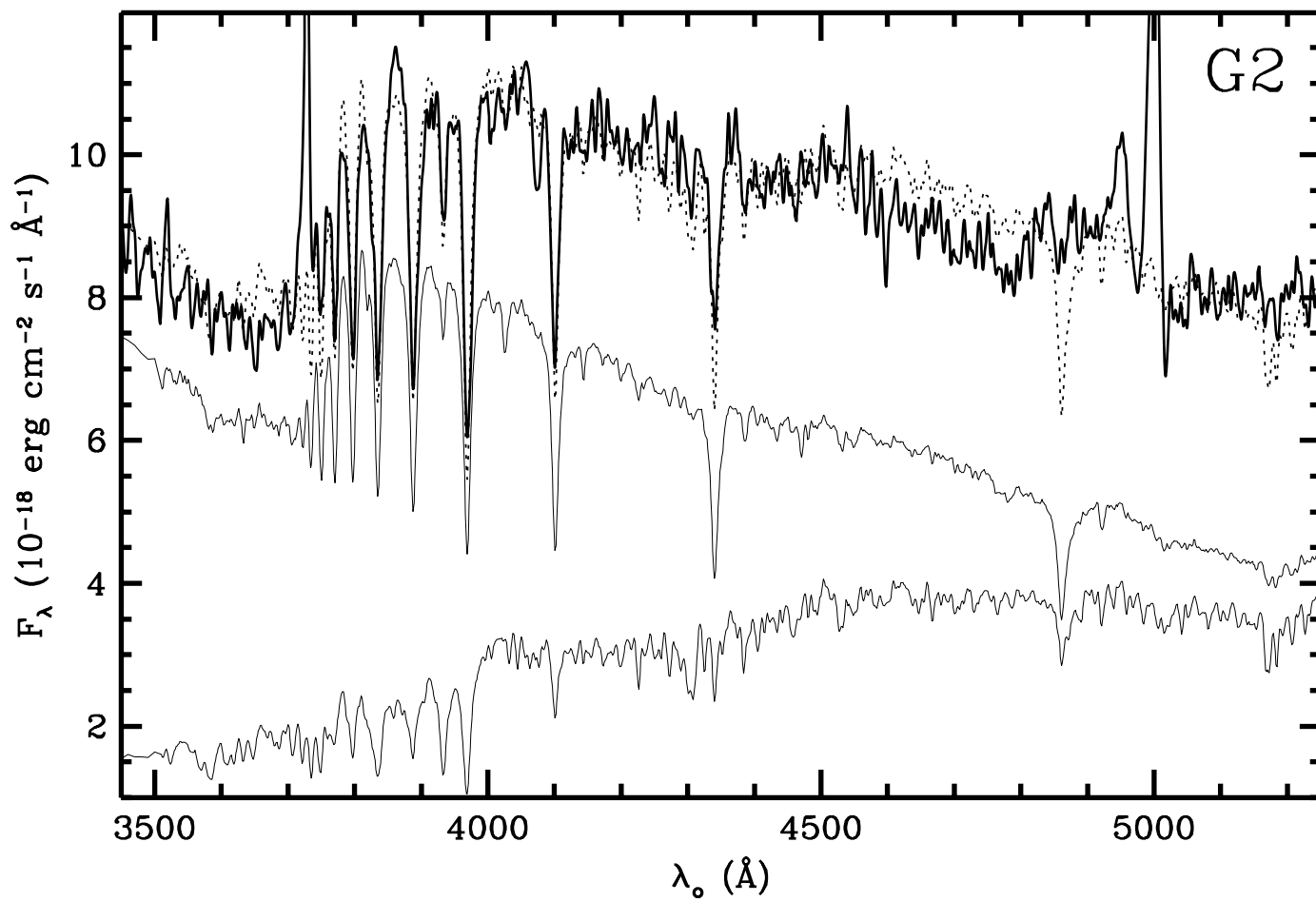
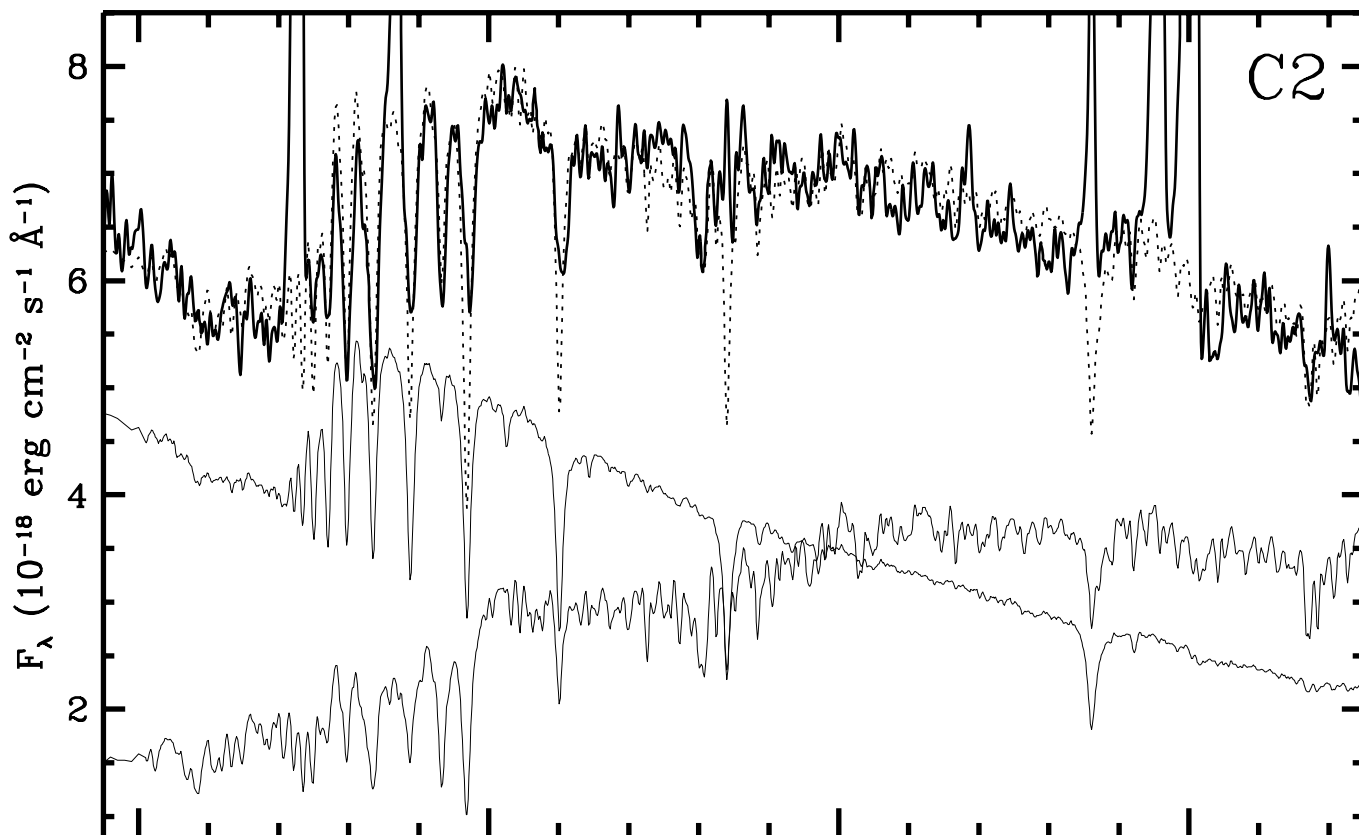
^cCanalizo, Stockton & Roth 1998

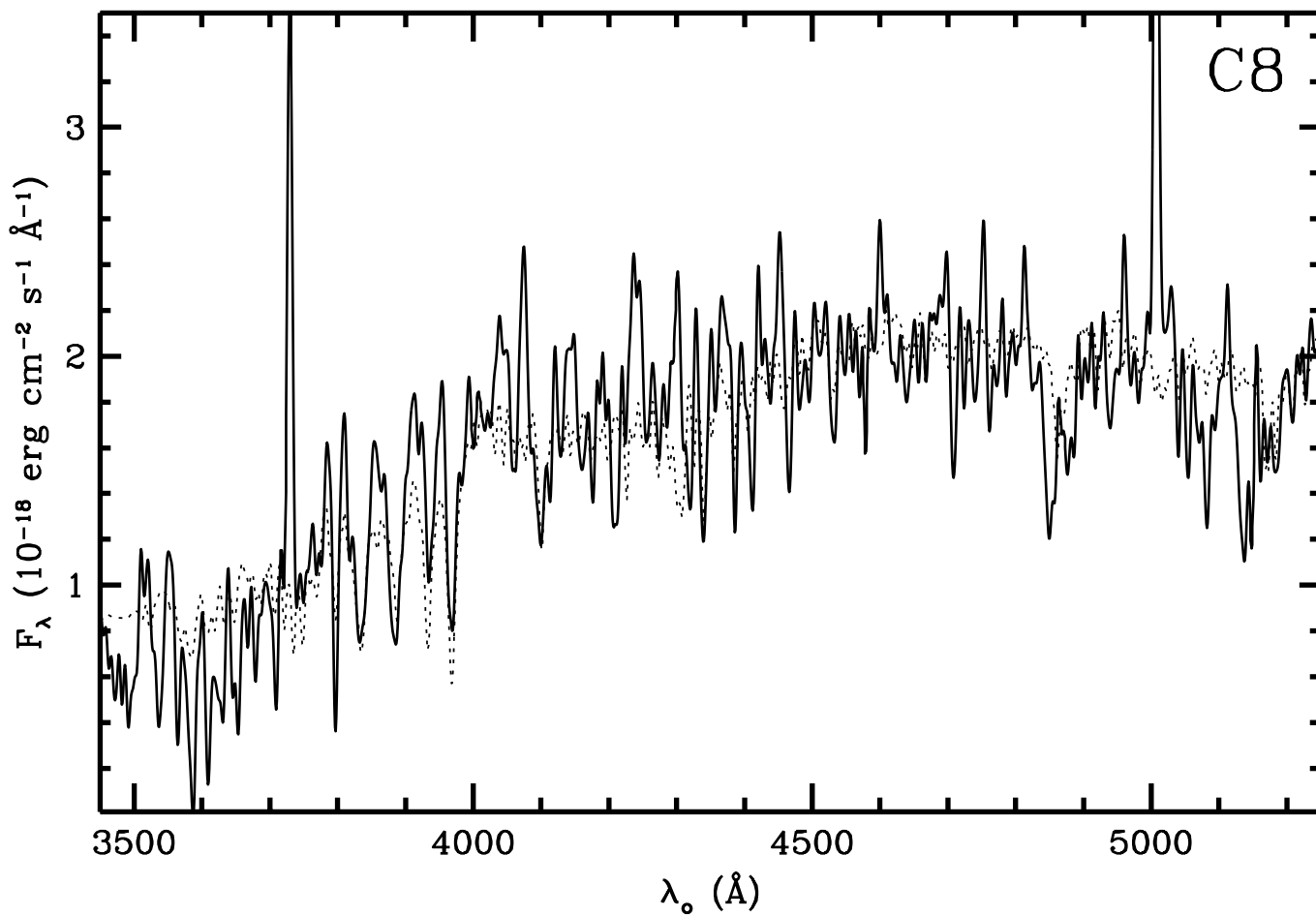
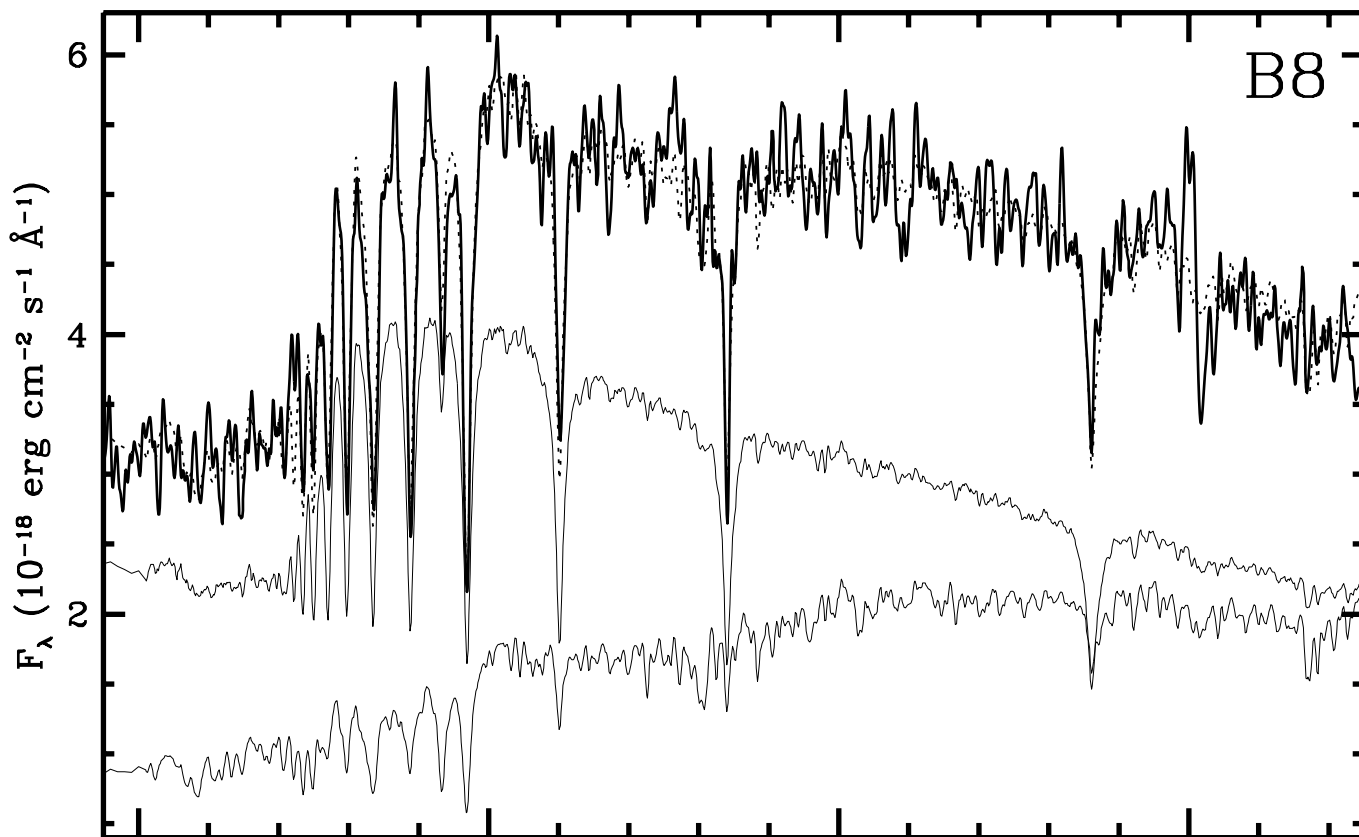


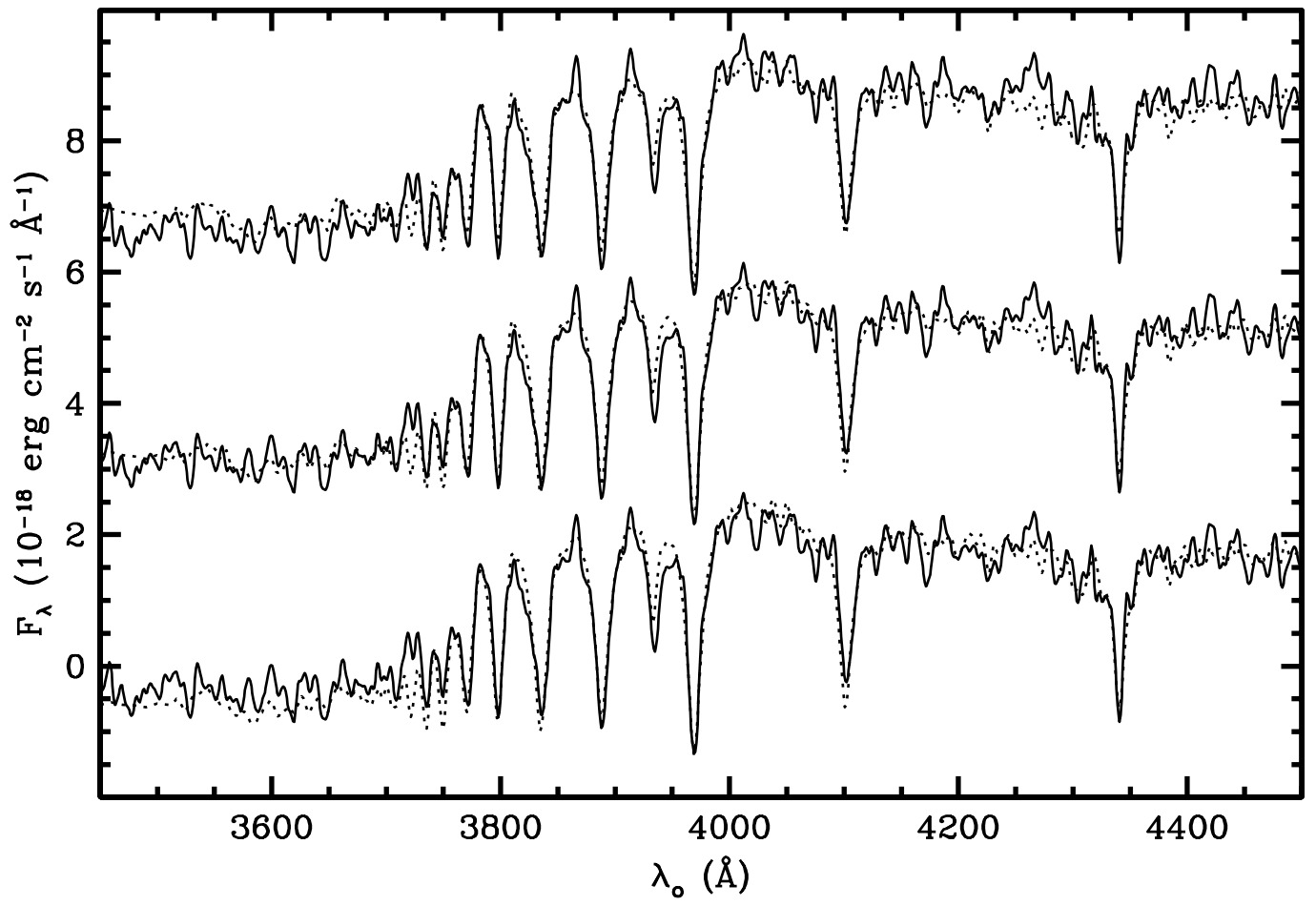
This figure "fig2.jpg" is available in "jpg" format from:

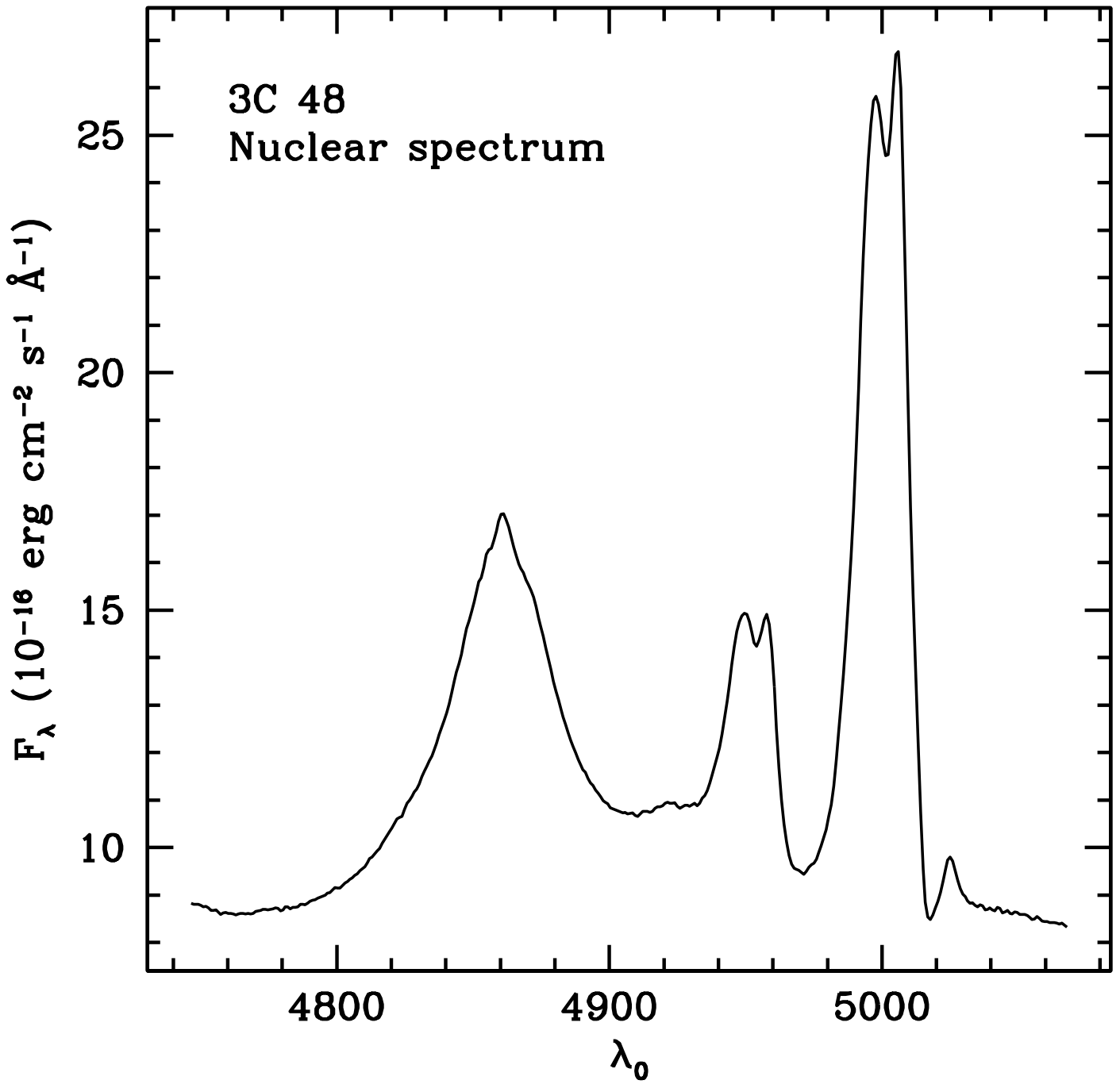
<http://arxiv.org/ps/astro-ph/9908020v1>











This figure "fig6.jpg" is available in "jpg" format from:

<http://arxiv.org/ps/astro-ph/9908020v1>

This figure "fig7.jpg" is available in "jpg" format from:

<http://arxiv.org/ps/astro-ph/9908020v1>

This figure "fig8.jpg" is available in "jpg" format from:

<http://arxiv.org/ps/astro-ph/9908020v1>

